Synthetic Gauge Fields in Synthetic Dimensions

A. Celi,[1] P. Massignan,[1] J. Ruseckas,[2] N. Goldman,[3] I. B. Spielman,[4,5] G. Juzeliūnas,[2] and M. Lewenstein[1,6]
[1]ICFO-Institut de Ciències Fotòniques, Mediterranean Technology Park, E-08860 Castelldefels (Barcelona), Spain
[2]Institute of Theoretical Physics and Astronomy, Vilnius University, A. Goštauto 12, Vilnius 01108, Lithuania
[3]Laboratoire Kastler Brossel, CNRS, UPMC, ENS, 24 rue Lhomond, F-75005 Paris, France
[4]Joint Quantum Institute, University of Maryland, College Park, Maryland 20742-4111, USA
[5]National Institute of Standards and Technology, Gaithersburg, Maryland 20899, USA
[6]ICREA-Institució Catalana de Recerca i Estudis Avançats, E-08010 Barcelona, Spain
(Received 2 September 2013; published 28 January 2014)

We describe a simple technique for generating a cold-atom lattice pierced by a uniform magnetic field. Our method is to extend a one-dimensional optical lattice into the "dimension" provided by the internal atomic degrees of freedom, yielding a synthetic two-dimensional lattice. Suitable laser coupling between these internal states leads to a uniform magnetic flux within the two-dimensional lattice. We show that this setup reproduces the main features of magnetic lattice systems, such as the fractal Hofstadter-butterfly spectrum and the chiral edge states of the associated Chern insulating phases.

DOI: 10.1103/PhysRevLett.112.043001 PACS numbers: 37.10.Jk, 03.75.Hh, 05.30.Fk

Intense effort is currently devoted to the creation of gauge fields for electrically neutral atoms [1–4]. Following a number of theoretical proposals in the presence [5–13] or in the absence of optical lattices [14–20], synthetic magnetic fields have been engineered both in vacuum [21–25] and in periodic lattices [26–29]. The addition of a lattice offers the advantage to realize extraordinarily large magnetic fluxes, of the order of 1 magnetic flux quantum per plaquette [5–7,10,11], which are out of reach using real magnetic fields in standard solid-state systems (see Refs. [30–34] for the realization of large fluxes in graphenelike and photonics systems). Such cold-atom lattice configurations will enable one to access striking properties, such as Hofstadter-like fractal spectra [35] and Chern insulating phases, in a controllable manner. Existing schemes for creating uniform magnetic fluxes require several laser fields and/or additional ingredients, such as tilted potentials [6,10], superlattices [11], or lattice-shaking methods [9,13,36–39]. Experimentally, strong staggered magnetic flux configurations have been reported [26,27], and very recently also uniform ones [28,29]. Besides, an alternative route is offered by optical flux lattices [40–43].

In all of these lattice schemes, the sites are identified by their location in space. This need not be the case: the available spatial degrees of freedom can be augmented by employing the internal atomic "spin" degrees of freedom. When three or more internal states are coupled in a sequential manner, one effectively obtains an extra, or synthetic, lattice dimension [44]. Here we demonstrate that this extra dimension can support a uniform magnetic flux, and we propose a specific scheme using a one-dimensional (1D) optical lattice along with Raman transitions within the atomic ground-state manifold (Fig. 1). The flux is produced by a combination of ordinary tunneling in real space and laser-assisted tunneling in the extra dimension creating the necessary Peierls phases. Our proposal therefore extends the toolbox of existing techniques to create gauge potentials for cold atoms [3,4]. The proposed scheme distinguishes itself by the naturally sharp boundaries in the extra dimension, a feature which greatly simplifies the detection of chiral edge states resulting from the synthetic magnetic flux [45–49]. We demonstrate that the chiral motion of these topological edge states can be directly visualized using *in situ* images of the cloud, and we explicitly show their robustness against impurity scattering. We also show that by using additional Raman and radio-frequency transitions one can connect the edges in the extra dimension, providing a remarkably simple way to realize the fractal Hofstadter-butterfly spectrum [35].

Model.—For specificity, consider ^{87}Rb's $F = 1$ ground-state hyperfine manifold [50], composed of three magnetic sublevels $m_F = 0, \pm 1$, illuminated by the combination of the optical lattice and Raman laser beams depicted in Fig. 1(a) (additional lattice potentials along $\mathbf{e}_y$ and $\mathbf{e}_z$ confining motion to $\mathbf{e}_x$ are not shown, and $\mathbf{e}_{xyz}$ are the three Cartesian unit vectors). In the schematic, the counterpropagating $\lambda = 1064$ nm lasers beams define the lattice with period $a = \lambda/2$, recoil momentum $k_L = 2\pi/\lambda$, and recoil energy $E_L = \hbar^2 k_L{}^2/2m$ (where m is the atomic mass). We consider a sufficiently deep lattice $V_{\mathrm{lat}} = 5E_L$ for the tight binding approximation to be valid, but shallow enough to avoid Mott-insulator physics. For these parameters, the tunneling amplitude is $t = 0.065E_L = h \times 133$ Hz. The Raman lasers at wavelength $\lambda_R \approx 790$ nm intersect with opening angle θ, giving an associated Raman recoil momentum $k_R = 2\pi \cos(\theta)/\lambda_R$. The Raman couplings recently exploited in experiment [21,22], between the three magnetic sublevels $m_F = 0, \pm 1$ of the $F = 1$ ground-state manifold of ^{87}Rb, are shown in Fig. 1(b). The Raman transitions provide the hopping in

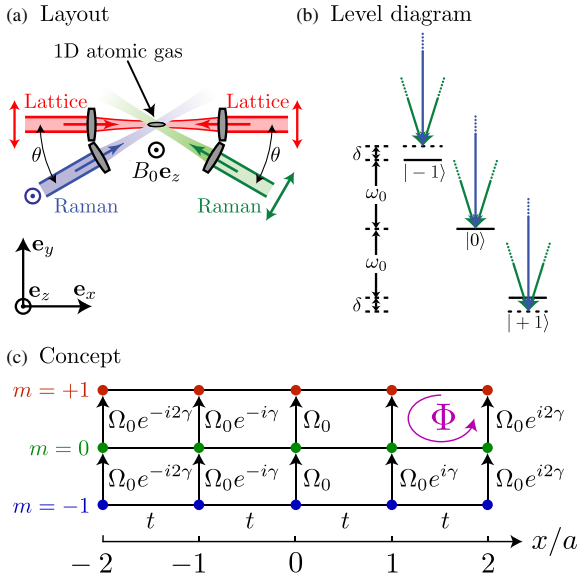

FIG. 1 (color online). (a) Proposed experimental layout with ^{87}Rb. A pair of counterpropagating $\lambda = 1064$ nm lasers provide a $5E_L$ deep optical lattice lattice with period $a = \lambda/2$. A pair of "Raman" laser beams with wavelength $\lambda_R = 790$ nm, at angles $\pm\theta$ from $\mathbf{e}_x$, couple the internal atomic states with recoil wave vector $k_R = 2\pi\cos(\theta)/\lambda_R$. The laser beams' polarizations all linear—are marked by symbols at their ends. (b) Raman couplings in the $F = 1$ manifold. The Raman lasers, far detuned from the electronic excited state, connect to the ground electronic states as indicated with the green and blue arrows [each coupling resulting from the like-colored laser beam in Fig. 1(a)]. (c) Synthetic 2D lattice with magnetic flux $\Phi = \gamma/2\pi$ per plaquette ($\gamma = 2k_R a$).

the synthetic dimension which require a minimum amount of laser light (less than 1% required for existing schemes [19]), minimizing spontaneous emission. In addition, periodic boundary conditions in the synthetic direction can be created by coupling $m_F = +1$ to $m_F = -1$ using an off-resonant Raman transition from $|F = 1, m_F = +1\rangle$ to an ancillary state, e.g., $|F = 2, m_F = 0\rangle$ (detuned by a frequency δ_{pbc} and coupled with strength $\Omega_{R,\mathrm{pbc}}$), completed by a radio-frequency transition to $|F = 1, m_F = 1\rangle$ with strength Ω_{RF}, giving a Λ-like scheme with strength $\Omega_{\mathrm{pbc}} = -\Omega_{R,\mathrm{pbc}}\Omega_{RF}/2\delta_{\mathrm{pbc}}$.

A constant magnetic field $B_0\mathbf{e}_z$ Zeeman splits the magnetic sublevels $|m_F = \pm 1\rangle$ by $\mp\hbar\omega_0 = g_F\mu_B B_0$, where g_F is the Landé g factor and μ_B is the Bohr magneton; see Figs. 1(a) and 1(b). We do not include the quadratic Zeeman effect, as it can be made negligible in a realistic experiment [51]. The Raman transitions, detuned by δ from two-photon resonance, impart a $2k_R$ recoil momentum along $\mathbf{e}_x$. Taking $\hbar = 1$, the laser fields can be described via an effective magnetic field

$$\Omega_T = \delta\mathbf{e}_z + \Omega_R[\cos(2k_R x)\mathbf{e}_x - \sin(2k_R x)\mathbf{e}_y], \quad (1)$$

which couples the hyperfine ground states giving the effective atom-light Hamiltonian [4,40,43,52]

$$H_{\mathrm{al}} = \Omega_T \cdot \mathbf{F} = \delta F_z + (F_+ e^{ik_R x} + F_- e^{-ik_R x})\Omega_R/2, \quad (2)$$

where the operators $F_\pm = F_x \pm iF_y$ act as $F_+|m\rangle = g_{F,m}|m+1\rangle$ with $g_{F,m} = \sqrt{F(F+1) - m(m+1)}$. Thus, the Raman beams sequentially couple states $m = -F, \ldots, F$, with each transition accompanied by an x-dependent phase. This naturally generates Peierls phases for "motion" along the m (spin) direction, denoted as $\mathbf{e}_m$.

The combination of the optical lattice along $\mathbf{e}_x$ and the Raman-induced hopping along $\mathbf{e}_m$ yields an effective two-dimensional (2D) lattice with one physical and one synthetic dimension, as depicted in Fig. 1(c) for $F = 1$. For a system of length L_x along $\mathbf{e}_x$, the lattice has $N = L_x/a$ sites along $\mathbf{e}_x$, and a width of $W = 2F + 1$ sites along $\mathbf{e}_m$. For $\delta = 0$ the system is described by the Hamiltonian

$$H = \sum_{n,m}(-ta^\dagger_{n+1,m} + \Omega_{m-1}e^{-i\gamma n}a^\dagger_{n,m-1})a_{n,m} + \mathrm{H.c.}, \quad (3)$$

where $n = x/a$ and m label, respectively, the spatial and spin indices, $\gamma = 2k_R a$ sets the magnetic flux, $\Omega_m = \Omega_R g_{F,m}/2$ is the synthetic tunneling strength, and $a^\dagger_{n,m}$ is the atomic creation operator in the extended lattice. This two-dimensional lattice is pierced by a uniform synthetic magnetic flux $\Phi = \gamma/2\pi = k_R a/\pi$ per plaquette (in units of the Dirac flux quantum). The quantity $g_{F,m}$ is independent of m for $F = 1/2$ and $F = 1$, but for larger F hopping along $\mathbf{e}_m$ is generally nonuniform.

Open boundaries.—Since $\Omega_m \neq 0$ only when $m \in \{-F, \ldots, F-1\}$, Eq. (3) has open boundary conditions along $\mathbf{e}_m$, with sharp edges at $m = \pm F$. By gauge transforming $a_{n,m}$ and $a^\dagger_{n,m}$, the hopping phase $\exp(i2k_R x)$ can be transferred to the hopping along $\mathbf{e}_x$. Combining this with a Fourier transformation along $\mathbf{e}_x$, $b^\dagger_{q,m} = N^{-1/2}\sum_{n=1}^{N} a^\dagger_{n,m}e^{i(q+\gamma m)n}$, splits the Hamiltonian $H = \sum_q H_q$ into momentum components

$$H_q = \sum_{m=-F}^{F} \varepsilon_{q+\gamma m} b^\dagger_{q,m} b_{q,m} + (\Omega_m b^\dagger_{q,m+1} b_{q,m} + \mathrm{H.c.}),$$

where $\varepsilon_k = -2t\cos(k)$, $q \equiv 2\pi l/N$, and $l \in \{1, \ldots, N\}$. Figure 2 shows the resulting band structure for $F = 1$. Away from the avoided crossings, the lowest band describes the propagation of "edge states" localized in spin space at $m = \pm F$ (blue and red arrows): these states propagate along $\mathbf{e}_x$ in opposite directions. In the physical system, these give rise to a spin current $j_s(x) = j_\uparrow - j_\downarrow$. When $W = 2F + 1 \gg 1$, these edge states become analogous to those in quantum Hall systems [51,53]. The $F = 9/2$ manifold of ^{40}K allows experimental access to this large-W limit [54], since its 10 internal states reproduce the Hofstadter-butterfly topological band structure.

The edge-state propagation can be directly visualized by confining a multicomponent Fermi gas to a region $x \in [-L_x/2, L_x/2]$ and by setting the Fermi energy E_{F} within the Raman-induced gap (dashed line in Fig. 2) [55]. In this

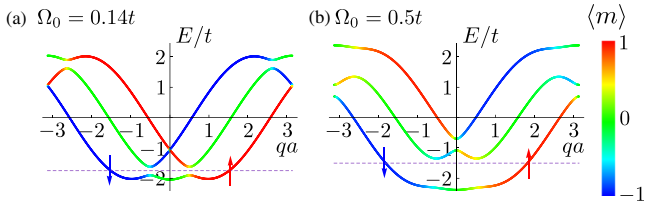

FIG. 2 (color online). Spectrum for open boundary conditions: $F = 1$ and $\Phi = \gamma/2\pi = 1/2\pi$ flux per plaquette. Colors specify the spin state m, i.e., blue, green, and red correspond to $m = -1, 0, 1$, respectively. The ground-state branch displays "edges" corresponding to $m = \pm 1$.

configuration, different types of states are initially populated: (a) edge states localized at $m = \pm F$ with opposite group velocities, and (b) bulk states delocalized in spin space with small group velocities (the central or bulk region of the lowest band is almost dispersionless for small flux $\Phi \ll 1$). When the confining potential along $\mathbf{e}_x$ is suddenly released, the edge states at $m = \pm F$ propagate along $\pm\mathbf{e}_x$. Figure 3 depicts such dynamics, where we allowed tightly confined atoms (as above) to expand into a harmonic potential $V_{\text{harm}}(x)$. This potential limits the propagation of the edge states along $\mathbf{e}_x$ and leads to chiral dynamics around the synthetic 2D lattice: when an edge state localized at $m = +F$ reaches the Fermi radius $x = R_F$, it cannot backscatter because of its chiral nature, and thus, it is obliged to jump on the other edge located at $m = -F$ and counterpropagate. At low energy, the lowest branch in Fig. 2(b) is separated from the two upper branches with a

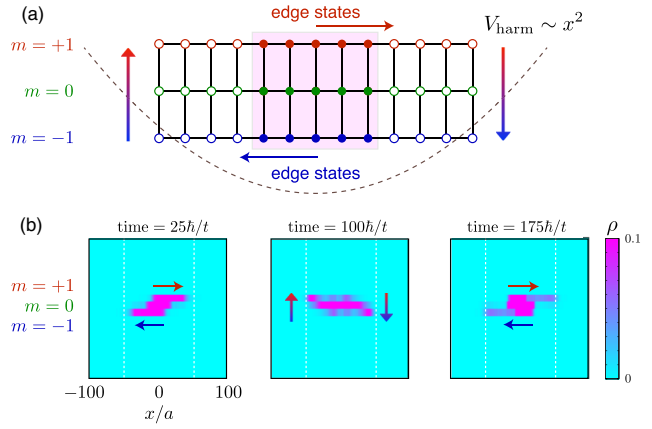

FIG. 3 (color online). Edge-state dynamics. (a) Initial condition: A Fermi gas is trapped in the central region $x \in [-13a, 13a]$ of a lattice with $\Omega_0 = 0.5t$, $\Phi = 1/2\pi$, and the Fermi energy $E_F = -1.4t$ is chosen to populate only the lowest energy band. The occupied edge states localized at $m = \pm F$ have opposite group velocities (for simplicity we sketch the $F = 1$ case). (b) Time-evolving density ρ after releasing the cloud into a harmonic potential $V_{\text{harm}}(x) = t(x/50a)^2$. The confinement limits the edge-state propagation and leads to chiral dynamics around the synthetic 2D lattice. Dashed white lines represent the Fermi radius R_F at which the edge states localized at $m = \pm F$ jump to the opposite edge $m = \mp F$.

gap of the order of the tunneling t, requiring temperatures ~nK to detect edge-state motion with given chirality [47,49,51]. The edge-state dynamics of a $F = 9/2$ lattice is shown in [51].

An interesting feature of edge states is their robustness against local perturbations. To check this in the context of our proposal, we consider the effects of a spatially localized impurity on the transmission probability T. The Hamiltonian with an impurity localized at $n = 0$ is

$$H_{\text{imp}} = H + V, \qquad V = \sum_m V_m a^\dagger_{0,m} a_{0,m}, \tag{4}$$

where the free Hamiltonian H is given in Eq. (3), and V_m models the interaction between the impurity and atoms in state m. The perturbation may be generated by a tightly focused laser, or by a distinguishable atom, deeply trapped by a species selective optical lattice [56–58]. If the impurity scatters equally strongly with all spin components, it corresponds to an extended obstacle along $\mathbf{e}_m$: a "roadblock" in the synthetic 2D lattice. On the other hand, if the impurity interacts significantly only with a given spin component, it yields a localized perturbation in the synthetic 2D lattice. In particular, edge perturbations can be engineered by choosing an impurity that only scatters strongly the $m = F$ or $m = -F$ states.

For $F = 1$ there are three dispersion branches, as shown in Fig. 2, so there are nine possible scattering channels. However, here we focus on the energy range lying inside the bulk gap (around the dashed lines in Fig. 2), where there is only one available scattering channel, i.e., scattering to the opposite edge state. The transmission as a function of the energy of the incident atom is calculated in [51] and shown in Fig. 4. For spin-independent collisions with the impurity ($V_m = U$), T goes to zero at two values of the energy within the gap. In analogy with Fano resonances [59,60], these zeros are associated with two quasibound states localized around the impurity potential due to two local parabolic minima (for $F = 1$) in the upper dispersion branches. Outside of the resonant regions, the transmission probability is close to 1. On the other hand, an impurity which scatters only the $m = 0$ component ($V_m = U\delta_{m,0}$) is effectively localized in the central chain of the synthetic 2D lattice. As such, it can couple resonantly two oppositely propagating edge states, leading to a single sharp minimum in the transmission probability. Instead, an impurity which is localized at the edge of the synthetic dimension (e.g., $V_m = U\delta_{m,1}$) does not lead to a resonant behavior of the transmission probability. For such spin-dependent impurity the transmission probability is always close to 1, since the edge state can go around the impurity in the synthetic dimension.

Cyclic couplings.—In the $F = 1$ case, periodic boundary conditions along $\mathbf{e}_m$ can be induced with an extra coupling (with a Rabi frequency $\Omega_1 = \Omega_{\text{pbc}} = \Omega_0$) from $|m = 1\rangle$ to $|m = -1\rangle$ accompanied by a momentum recoil k along $\mathbf{e}_x$. The system becomes periodic once the flux γ per plaquette is rational, i.e., $\gamma = 2\pi P/Q$ with P, Q coprime integers.

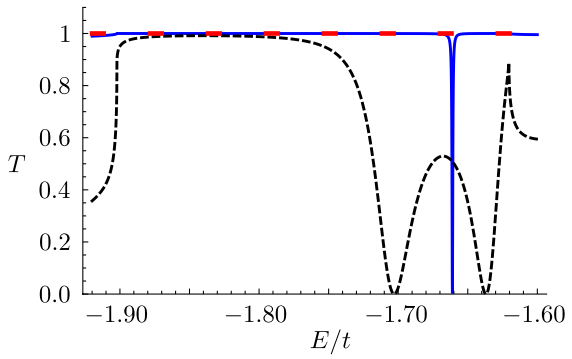

FIG. 4 (color online). Edge-state transmission probability. Short dashes (black): A spin-independent impurity. Solid (blue): Only $m = 0$ scatters. Long dashes (red): Only $m = 1$ scatters. Parameters are the same as in Fig. 2(a) and the scattering strength is $U = -t$.

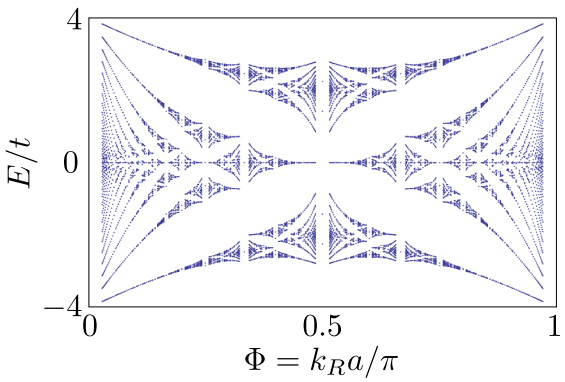

FIG. 5 (color online). The spectrum of Eq. (5) on an infinite 1D chain, for a three-level system with closed boundary conditions has the typical Hofstadter-butterfly characteristics.

Periodicity requires the number of loops in the synthetic dimension to be l/M, where l is the least common multiple of M and Q, thus, for $M = 3$, Q, or $Q/3$ loops.

In this cyclic scheme, the system reproduces the Hofstadter problem defined in the infinite plane: its spectrum $E = E(p)$ is obtained by solving the Harper equation along $\mathbf{e}_x$ [54], where p is the quasimomentum associated with the closed synthetic dimension $\mathbf{e}_y$. The conserved momentum along $\mathbf{e}_y$ can only take three values: $p_j = 2\pi j/3$ with $j \in \{-1, 0, 1\}$. Exploiting the fact that the Hamiltonian (3) with closed boundary conditions is translationally invariant in the spin dimension, we perform the Fourier transform $a^\dagger_{n,m} = 3^{-1/2} \sum_{j=-1}^{1} e^{i2\pi mj/3} c^\dagger_{n,j}$, giving

$$H = \sum_{j,n} \epsilon(2\pi j/3 + n\gamma) c^\dagger_{n,j} c_{n,j} - (t c^\dagger_{n+1,j} c_{n,j} + \text{H.c.}) \quad (5)$$

and $\epsilon(k) = -2\Omega_0 \cos(k)$. Its spectrum is plotted in Fig. 5. There are l points in each band associated with the rational flux γ, enough to be visible. For our finite chain of length N, the infinite-chain result will be accurate only for $Q \ll N$, while for Q approaching N the system is far from periodic in Q and the butterfly gets blurred.

Interactions.—We consider the effects of repulsive interactions, focusing on the case where those are SU(W) invariant (this amounts to neglecting the spin-dependent contribution to the interaction, a very good approximation for $F = 1$ ^{87}Rb). In our lattice, the resulting interaction Hamiltonian

$$H_{\text{int}} = \frac{\mathcal{U}}{2} \sum_n \mathcal{N}_n(\mathcal{N}_n - 1), \qquad \mathcal{N}_n \equiv \sum_m a^\dagger_{n,m} a_{n,m},$$

is local along $\mathbf{e}_x$, but infinite in range along $\mathbf{e}_m$. We exploit the SU(W) invariance of H_{int} by adopting the Fock basis $c_{n,j}$ in which the hopping along $\mathbf{e}_m$ is diagonal, as in Eq. (5) (a similar basis exists for open boundary conditions in the synthetic dimension). Let us denote its eigenvalues by $\epsilon_{n,j}$. We can minimize the energy for fixed $\langle H_{\text{int}} \rangle$ by populating only the states associated to c_{n,j_n} with lowest ϵ_{n,j_n}, as this minimizes the kinetic term $\langle H \rangle$.

Two cases are possible: (i) j_n is unique, i.e., the local ground state is not degenerate; (ii) $\epsilon_{j,n}$ is minimal for two of the three possible values of j. The latter case can occur only for closed boundary conditions in the synthetic dimension and for rational values of the flux $\gamma/(2\pi) = P/Q$. In the presence of open boundary conditions, it is indeed easy to show that the eigenvalues are always independent of γ (and therefore of n), and never degenerate. In case (i), the ground state can be mapped to one of a 1D uniform Bose-Hubbard chain. In case (ii) instead, the 1D Hubbard chain will possess a primitive cell containing Q consecutive lattice points, as is well known from the noninteracting Hofstadter problem. Interactions which are non-SU(W) invariant lead to considerably more complicated situations, with the ground state possessing a complex, fully 2D character.

Conclusions.—Our proposal for creating strong synthetic gauge fields using a synthetic 2D lattice is well suited to directly observe chiral edge-state dynamics, by using spin-sensitive detection of the different edge modes. This platform also allows us to test the edge states' robustness against impurities. The complete Hofstadter spectrum can be detected either with bosons or fermions. Interaction effects shall be kept at reasonably small values, e.g., by using a dilute thermal gas of bosons, or a degenerate Fermi gas far from any Feshbach resonances. As the Hofstadter spectrum is symmetric around $E = 0$, its mapping may be obtained by investigating systems at band filling less than $1/2$, thereby avoiding, e.g., strong interaction effects arising in fermionic systems close to unit filling [61]. The spectrum may also be probed by transport measurements: wave packets with narrow energy dispersion can be prepared and brought into the lattice using a waveguide, and their transmission through the region of effective magnetic field observed [62,63].

We acknowledge enlightening discussions with E. Anisimovas, F. Chevy, J. Dalibard, L. Fallani, F. Gerbier,

and C. Salomon and support from FRS-FNRS (Belgium) and Université Libre de Bruxelles (ULB), ERC AdG QUAGATUA, EU IP SIQS, EU STREP EQuaM, Spanish MINCIN (FIS2008-00784 TOQATA), ESF POLATOM, the European Social Fund under the Global Grant measure. I. B. S. acknowledges the support of the ARO with funding from DARPA's OLE program and the Atomtronics-MURI; and the NSF through the PFC at JQI.

[1] M. Lewenstein, A. Sanpera, V. Ahufinger, B. Damski, A. Sen(De), and U. Sen, Adv. Phys. **56**, 243 (2007).
[2] I. Bloch, J. Dalibard, and W. Zwerger, Rev. Mod. Phys. **80**, 885 (2008).
[3] J. Dalibard, F. Gerbier, G. Juzeliūnas, and P. Öhberg, Rev. Mod. Phys. **83**, 1523 (2011).
[4] N. Goldman, G. Juzeliūnas, P. Öhberg and I. B. Spielman, arXiv:1308.6533.
[5] J. Ruostekoski, G. V. Dunne, and J. Javanainen, Phys. Rev. Lett. **88**, 180401 (2002).
[6] D. Jaksch and P. Zoller, New J. Phys. **5**, 56 (2003).
[7] E. J. Mueller, Phys. Rev. A **70**, 041603 (2004).
[8] A. S. Sørensen, E. Demler, and M. D. Lukin, Phys. Rev. Lett. **94**, 086803 (2005).
[9] A. Eckardt, C. Weiss, and M. Holthaus, Phys. Rev. Lett. **95**, 260404 (2005).
[10] K. Osterloh, M. Baig, L. Santos, P. Zoller, and M. Lewenstein, Phys. Rev. Lett. **95**, 010403 (2005).
[11] F. Gerbier and J. Dalibard, New J. Phys. **12**, 033007 (2010).
[12] T. Kitagawa, E. Berg, M. Rudner, and E. Demler, Phys. Rev. B **82**, 235114 (2010).
[13] A. R. Kolovsky, Europhys. Lett. **93**, 20003 (2011).
[14] R. Dum and M. Olshanii, Phys. Rev. Lett. **76**, 1788 (1996).
[15] P. M. Visser and G. Nienhuis, Phys. Rev. A **57**, 4581 (1998).
[16] G. Juzeliūnas and P. Öhberg, Phys. Rev. Lett. **93**, 033602 (2004).
[17] J. Ruseckas, G. Juzeliūnas, P. Öhberg, and M. Fleischhauer, Phys. Rev. Lett. **95**, 010404 (2005).
[18] G. Juzeliūnas, J. Ruseckas, P. Öhberg, and M. Fleischhauer, Phys. Rev. A **73**, 025602 (2006).
[19] I. B. Spielman, Phys. Rev. A **79**, 063613 (2009).
[20] K. J. Günter, M. Cheneau, T. Yefsah, S. P. Rath, and J. Dalibard, Phys. Rev. A **79**, 011604 (2009).
[21] Y.-J. Lin, R. L. Compton, K. Jiménez-García, J. V. Porto, and I. B. Spielman, Nature (London) **462**, 628 (2009).
[22] Y.-J. Lin, R. L. Compton, A. R. Perry, W. D. Phillips, J. V. Porto, and I. B. Spielman, Phys. Rev. Lett. **102**, 130401 (2009).
[23] L. J. LeBlanc, K. Jiménez-García, R. A. Williams, M. C. Beeler, A. R. Perry, W. D. Phillips, and I. B. Spielman,, Proc. Natl. Acad. Sci. U.S.A. **109**, 10811 (2012).
[24] P. Wang, Z.-Q. Yu, Z. Fu, J. Miao, L. Huang, S. Chai, H. Zhai, and J. Zhang, Phys. Rev. Lett. **109**, 095301 (2012).
[25] L. W. Cheuk, A. T Sommer, Z. Hadzibabic, T. Yefsah, W. S. Bakr, and M. W. Zwierlein, Phys. Rev. Lett. **109**, 095302 (2012).
[26] M. Aidelsburger, M. Atala, S. Nascimbène, S. Trotzky, Y.-A. Chen, and I. Bloch, Phys. Rev. Lett. **107**, 255301 (2011).
[27] J. Struck *et al.*, Nat. Phys. **9**, 738 (2013).
[28] M. Aidelsburger, M. Atala, M. Lohse, J. T. Barreiro, B. Paredes, and I. Bloch, Phys. Rev. Lett. **111**, 185301 (2013).
[29] H. Miyake, G. A. Siviloglou, C. J. Kennedy, W. C. Burton, and W. Ketterle, Phys. Rev. Lett. **111**, 185302 (2013).
[30] L. A. Ponomarenko *et al.*, Nature (London) **497**, 594 (2013).
[31] C. R. Dean *et al.*, Nature (London) **497**, 598 (2013).
[32] B. Hunt *et al.*, Science **340** 1427 (2013).
[33] M. C. Rechtsman, Y. Plotnik, J. M. Zeuner, D. Song, Z. Chen, A. Szameit, and M. Segev, Phys. Rev. Lett. **111**, 103901 (2013).
[34] M. Hafezi, S. Mittal, J. Fan, A. Migdall, and J. M. Taylor, Nat. Photonics **7**, 1001 (2013).
[35] D. R. Hofstadter, Phys. Rev. B **14**, 2239 (1976).
[36] A. Zenesini, H. Lignier, D. Ciampini, O. Morsch, and E. Arimondo, Phys. Rev. Lett. **102**, 100403 (2009).
[37] A. Eckardt, P. Hauke, P. Soltan-Panahi, C. Becker, K. Sengstock, and M. Lewenstein, Europhys. Lett. **l89**, 10010 (2010).
[38] J. Struck, C. Olschlager, R. Le Targat, P. Soltan-Panahi, A. Eckardt, M. Lewenstein, P. Windpassinger, and K. Sengstock, Science **333**, 996 (2011).
[39] P. Hauke *et al.*, Phys. Rev. Lett. **109**, 145301 (2012).
[40] A. M. Dudarev, R. B. Diener, I. Carusotto, and Q. Niu, Phys. Rev. Lett. **92**, 153005 (2004).
[41] N. Cooper, Phys. Rev. Lett. **106**, 175301 (2011).
[42] N. R. Cooper and J. Dalibard, Europhys. Lett. **95**, 66004 (2011).
[43] G. Juzeliūnas and I. B. Spielman, New J. Phys. **14**, 123022 (2012).
[44] O. Boada, A. Celi, J. I. Latorre, and M. Lewenstein, Phys. Rev. Lett. **108**, 133001 (2012).
[45] N. Goldman, I. Satija, P. Nikolic, A. Bermudez, M. A. Martin-Delgado, M. Lewenstein, and I. B. Spielman, Phys. Rev. Lett. **105**, 255302 (2010).
[46] T. D. Stanescu, V. Galitski, and S. D. Sarma, Phys. Rev. A **82**, 013608 (2010).
[47] N. Goldman, J. Beugnon, and F. Gerbier, Phys. Rev. Lett. **108**, 255303 (2012).
[48] M. Buchhold, D. Cocks, and W. Hofstetter, Phys. Rev. A **85**, 063614 (2012).
[49] N. Goldman, J. Dalibard, A. Dauphin, F. Gerbier, M. Lewenstein, P. Zoller, and I. B. Spielman, Proc. Natl. Acad. Sci. U.S.A. **110**, 6736 (2013).
[50] While our discussion focuses on ^{87}Rb atoms with $F = 1$, the general principle is applicable to any cold-atom systems where a number of internal states can be consecutively Raman coupled.
[51] See Supplemental Material at http://link.aps.org/supplemental/10.1103/PhysRevLett.112.043001 for an expanded discussion of the experimental issues and of the edge-state physics for $F > 1$, and for the detailed calculation of scattering by impurities.
[52] I. H. Deutsch and P. S. Jessen, Phys. Rev. A **57**, 1972 (1998).
[53] D. Hügel and B. Paredes, arXiv:1306.1190.
[54] Y. Hatsugai, Phys. Rev. Lett. **71**, 3697 (1993).
[55] Note that the "$F = 1$" Fermi system sketched in Figs. 2–3 could be realized by coupling three spin states of fermionic ^{40}K or ^{173}Yb. L. Fallani (private communication).
[56] P. Massignan and Y. Castin, Phys. Rev. A **74**, 013616 (2006).
[57] Y. Nishida and S. Tan, Phys. Rev. Lett. **101**, 170401 (2008).

[58] G. Lamporesi, J. Catani, G. Barontini, Y. Nishida, M. Inguscio, and F. Minardi, Phys. Rev. Lett. **104**, 153202 (2010).
[59] U. Fano, Phys. Rev. **124**, 1866 (1961).
[60] A. M. Satanin and Y. S. Joe, Phys. Rev. B **71**, 205417 (2005).
[61] J. Kajala, F. Massel, and P. Törmä, Phys. Rev. Lett. **106**, 206401 (2011).
[62] T. Lauber, P. Massignan, G. Birkl, and A. Sanpera, J. Phys. B **44**, 065301 (2011).
[63] P. Cheiney, F. Damon, G. Condon, B. Georgeot, and D. Guéry-Odelin, Europhys. Lett. **103**, 50006 (2013).